Energy Conversion and Management 127 (2016) 504–514

Contents lists available at ScienceDirect

Energy Conversion and Management

journal homepage: www.elsevier.com/locate/enconman

Numerical study of pyrolysis oil combustion in an industrial gas turbine

J.L.H.P. Sallevelt, A.K. Pozarlik *, G. Brem

University of Twente, Department of Energy Technology, Drienerlolaan 5, 7522 NB Enschede, The Netherlands

ARTICLE INFO

Article history:
Received 18 April 2016
Received in revised form 7 September 2016
Accepted 8 September 2016
Available online 19 September 2016

Keywords:
CFD
Spray combustion
Multicomponent biofuels
Pyrolysis oil
Evaporation

ABSTRACT

The growing demand for the use of biofuels for decentralized power generation initiates new research in gas turbine technology. However, development of new combustors for low calorific fuels is costly in terms of time and money. To give momentum to biofuels application for power generation robust numerical models for multicomponent biofuels must be developed. This paper discusses the use of CFD techniques for modeling the combustion of pyrolysis oil in a new burner geometry from OPRA Turbines. Pyrolysis oil contains many different compounds, which are represented by a discrete fuel model consisting of seven components. The components and their initial fractions approximate the volatility, water content, elemental composition and heating value of a typical fast pyrolysis oil. Simulations have been carried out for both the multicomponent pyrolysis oil and, as a reference, ethanol, a single-component biofuel with a higher volatility. Comparative simulations have been performed to examine the influence of the initial droplet size and to evaluate different combustion models. The results were compared to available experimental data for pyrolysis oil and ethanol combustion. A qualitatively good agreement was achieved.

1. Introduction

Fast pyrolysis oil is a renewable biofuel produced from biomass waste materials that can potentially be used as a fuel for industrial applications [1–10]. It is composed of a large number of oxygenated compounds that are formed during the thermal decomposition of biomass in the pyrolysis process. The chemical and physical properties of pyrolysis oil are markedly different from conventional fossil fuels [11–13]. Regarding spray combustion applications, the high water content, high viscosity and high coking tendency are particularly challenging. Several test campaigns have indicated that these properties can cause incomplete combustion and fouling [4,14–16]. It is generally concluded that modification of the combustion equipment is required to achieve acceptable operating performance with this biofuel.

The development of new combustors for this purpose can be facilitated by models that describe the evaporation and burning characteristics of pyrolysis oil with respect to other fuels. Especially CFD models can be useful to gain insight into the interactions between the pyrolysis oil spray and the surrounding air in a combustion chamber. However, the numerical analysis of these phenomena has received little attention so far. Only a few models have been proposed to approximate the behavior of pyrolysis oil droplets in a high temperature environment [17–24]. Since most of these models are restricted to the evaporation process, the characterization of the entire combustion process using numerical methods still needs to be explored.

This paper presents a CFD approach for modeling pyrolysis oil spray combustion in an industrial gas turbine. The commercial code ANSYS Fluent has been employed to model the vaporization and combustion of pyrolysis oil in the low-caloric fuel combustor that was recently developed by OPRA for the application of biofuels in their OP16 gas turbine [22]. The aim is to capture the main burning characteristics of pyrolysis oil. The results have been compared to simulations with ethanol, a single-component biofuel. Additional computations have been performed to verify the sensitivity of the results to the initial droplet size and to the combustion model. Although the detailed experimental data regarding flow and temperature field at various locations inside the combustor, as well as droplet size and distribution were not available for validation purpose, the model outcome was compared to experimental exhaust gas temperature and CO_2 emissions. Comparison with outlet measurements is frequently performed in case the detailed data regarding specific flow profiles is out of reach current experimental techniques, see [25–28].

2. Pyrolysis oil fuel model

Considering the large number of compounds present in pyrolysis oil, the composition was simplified using a discrete component

* Corresponding author.
E-mail address: a.k.pozarlik@utwente.nl (A.K. Pozarlik).

http://dx.doi.org/10.1016/j.enconman.2016.09.029
0196-8904/

approach. To capture the most relevant properties for the evaporation and combustion behavior, a surrogate fuel was developed that represents the volatility, water content, elemental composition and heating value of a typical pyrolysis oil.

The pyrolysis oil devolatilization characteristics reported by Branca et al. [23] were used as a guideline in selecting the components for the fuel model. On basis of thermogravimetric analysis (TGA) of four different pyrolysis oils (BTG, Dynamotive, Ensyn and Pyrovac), they proposed to divide the devolatilization curve into six main temperature zones. It was shown that the measured weight loss in the zones could be correlated with the mass fractions of the compounds identified in the oil samples of which the boiling points fell within the corresponding temperature ranges. In the surrogate fuel developed for the current 37 study, the total weight loss in each of the six temperature zones is lumped into a single organic compound that is typically found in pyrolysis oils. Water has been selected as an additional species, because it is the most abundant constituent of pyrolysis oil and highly influences the evaporation curve due to its high latent heat of vaporization. This approach resulted in the fuel model specified in Table 1. The surrogate fuel has an elemental composition of C 40% H 8.5% O 51% by weight and a lower heating value (LHV) of 15.6 MJ/kg, both of which are typical for fast pyrolysis oils [24,29–31].

The initial mass fractions of the surrogate fuel components have been estimated by evaluating TGA data reported in the literature. Branca et al. [23] determined devolatilization curves for the above-mentioned pyrolysis oils using a heating rate of 5 K/min up to a final temperature of 600 K. The measured weight loss in each of the six temperature zones was compared to their prediction for the mass loss in the zones. These predictions were based on the mass fractions of the oil constituents that were allocated to the zone based on their boiling points.

For the Dynamotive and BTG oils, the TGA data obtained from these experiments are listed alongside the predictions in Table 2. Both oils were produced from softwood and obtained by collecting the entire liquid from the pyrolysis reactor. Due to differences in the feedstock and the production process, the Ensyn and Pyrovac oils were considerably less volatile and therefore excluded from the present discussion. Table 2 also shows the TGA results reported by Van Rossum et al. [30]. These experiments were performed with pyrolysis oil produced from forest residue by VTT using a heating rate of 50 K/min up to an oil temperature of 823 K. The latter two columns in the table show TGA data for the same VTT oil, but the reported temperatures are of the sample cup in those cases.

The weight loss of the Dynamotive and BTG oils measured by Branca et al. deviates considerably from the predictions, especially in the lowest temperature zones. It was stated that these differences were mainly caused by the low heating rate used for the analysis. The slow process presumably allowed the oil constituents to largely evaporate already before their respective boiling points were reached. A reasonable agreement between the measurements and predictions for the individual oils was however observed by comparing the total weight loss over the first three zones, which cover the evaporation of water and all relatively light compounds.

A comparison of the TGA data obtained for the two oils shows that the BTG oil is more volatile than the Dynamotive oil in the lower temperature regions. The primary reasons for the higher volatility are the higher water content (30 vs 21 wt.%) and the lower pyrolytic lignin fraction (8 vs 25 wt.%) of the BTG oil. The TGA curve obtained for the VTT oil with a water content of 24 wt.% and a heating rate of 50 K/min is generally similar to that of the BTG oil. A large difference is seen in the highest temperature zone, however, presumably because the VTT sample was heated to a higher final temperature.

Table 1
Specification of the discrete fuel model used as a surrogate for pyrolysis oil. The temperature zones have been adopted from Branca et al. [23]. T_b and Y_{init} denote respectively the boiling point and the initial mass fraction.

Zone	Oil temperature (K)	Component	Formula	T_b (K)	Y_{init} (%)
1	<360	Methanol	CH_3OH	338	10
2	360–400	Water	H_2O	373	25
		Acetic acid	CH_3COOH	391	10
3	400–450	Acetol	$C_3H_6O_2$	419	10
4	450–500	Phenol	C_6H_5OH	455	10
5	500–550	Eugenol	$C_{10}H_{12}O_2$	527	15
6	>550	Levoglucosan	$C_6H_{10}O_5$	623	20

Table 2
Weight loss (WL) in wt.% for the different temperature zones as measured using TGA. Predictions are based on oil composition and boiling points. Data reproduced from Branca et al. [23] and from Van Rossum et al. [30].

Zone	Temp. zone (K)	WL vs T_{oil}					WL vs T_{cup}	
		Dynamotive[a]		BTG[b]		VTT[c]	VTT[d]	VTT[e]
		TGA	Pred.	TGA	Pred.	TGA	TGA	TGA
1	<360	16.7	7.8	27.6	7.9	28.0	28	7
2	360–400	13.3	33.2	16.6	44.4	18.4	15	17
3	400–450	13.7	8.4	13.1	6.5	9.6	11	16
4	450–500	9.7	2.9	8.3	1.6	7.0	8	10
5	500–550	8.9	4.7	5.7	3.1	5.0	4	9
6	>550	6.0	7.2	4.2	4.9	16.0	16	26
1–2	<400	30	41	44	52	46	43	24
1–3	<450	44	49	57	59	56	54	40
1–6	Full range	68	64	76	68	84	82	85

[a] Dynamotive oil, 21% water, heating rate 5 K/min up to 600 K based on oil temperature.
[b] BTG oil, 30% water, heating rate 5 K/min up to 600 K based on oil temperature.
[c] VTT oil, 24% water, heating rate 50 K/min up to 823 K based on oil temperature. Predictions are not available.
[d] VTT oil, 24% water, heating rate 1 K/min up to 1073 K based on sample cup temperature.
[e] VTT oil, 24% water, heating rate 100 K/min up to 1073 K based on sample cup temperature.

Since the heating rates in a gas turbine combustor are several orders of magnitude higher (typically $\geqslant 10^5$ K/min), the actual evaporation curve of a droplet in the spray is expected to approach the extreme case of sequential boiling more closely than seen in Table 2. This presumption is supported by TGA measurements at different heating rates conducted by Van Rossum et al. [30]. In Table 2, the measured weight loss of the VTT oil in each zone is reported for heating rates of 1 and 100 K/min up to a temperature of 1073 K based on the sample cup temperature. The data cannot be directly compared to the other values given in the table because the temperature of the pyrolysis oil itself is unknown, but the results indicate that the release of volatiles is shifted towards higher temperatures in case the heating rate is increased. It therefore seems plausible that the evaporation behavior at high heating rates will be strongly correlated with the oil composition and the boiling points of the various components.

Following these considerations, the initial weight fractions for the lowest three temperature zones given in Table 1 ($T < 450$ K) have been chosen based on the predicted values reported in Table 2. The total mass fraction represented by these zones was constrained to 55%, which is the average value of the predictions for the Dynamotive and BTG oils. After setting the water content to 25 wt.%, the average value of all three oils considered in the table, the remaining mass was divided over the other three components in these zones.

For the higher temperature zones ($T > 450$ K), the data in Table 2 cannot be used as a reliable basis for the present fuel model. Firstly, the chemical characterization of the oils was incomplete regarding the heavier species. It can be seen that the predicted values do not sum up to 100%, which is mainly because the nonvolatile fractions were excluded from the analysis [32]. Secondly, the TGA results obtained at such temperatures are not representative because the liquid phase chemistry is sensitive to the heating rate. At low heating rates (1–100 K/min), pyrolysis oils show a high tendency to form nonvolatile material under influence of polymerization reactions once the water and light components have evaporated [30]. This polymerization process typically results in a large amount of secondary char at the end of a TGA experiment, as can be seen from the total weight loss data given in Table 2. In several studies, however, it was observed that the charring tendency of pyrolysis oil is strongly reduced by increasing the heating rate. Evaporation experiments with small droplets resulted in a char yield as low as 4% [30] and 1% [31] of the original pyrolysis oil mass. The heating rates in these experiments were estimated to be 10^6 and above 10^5 K/min, respectively. In spray combustion experiments only 0.1% of the original mass was obtained as char [33], although it must be noticed that the hot product gases were not quenched so that part of the char could have been consumed via surface reactions. Nevertheless, these studies clearly show that TGA underpredicts the mass release in the upper temperature regions.

Given the low char yield under typical spray combustion conditions, a solid phase was not included in the fuel model. The small amounts of char that remain from the droplets may have implications for the soot emission and the service life of certain engine components, but are not expected to significantly influence the general combustion characteristics currently studied. Consequently, the initial mass fractions chosen for the components in zones 4–6 in Table 1 account for the evaporation of volatiles with a high boiling point as well as the cracking of the nonvolatile pyrolysis oil constituents. As the content of nonvolatiles (pyrolytic lignin, sugars, extractives) is very significant in most oils [29,34,35], the mass fractions are increasing towards higher boiling points. However, it remains uncertain if the assumed fractions accurately describe the evaporation curve in this region because reference data is not available. As the pyrolytic lignin largely consists of macromolecules with unknown properties, levoglucosan is chosen as the heaviest component in the oil. Levoglucosan is a major compound in pyrolysis oils and can imitate the fact that the lignin does not evaporate or decompose until a high droplet temperature is reached.

The properties of the seven fuel components in the model have largely been found in the Fluent built-in database, in other property databases [36–39] or in the literature [40–45]. Property data that were not directly available have been estimated using methods proposed in the literature [40,46–49].

3. Numerical methods

The combustion of pyrolysis oil and ethanol in an industrial gas turbine burner has been numerically investigated by using the Euler Lagrange RANS approach in ANSYS Fluent 14.5 [50]. The numerical setup for ethanol combustion is partly based on the modeling approach discussed in Sallevelt et al. [51] for the combustion of ethanol in a conventional diffusion-mode burner.

3.1. Computational domain

Fig. 1 shows a schematic of the combustion chamber that is considered in this study. This reverse-flow tubular combustor has recently been developed by OPRA Turbines to efficiently burn low-calorific fuels in the OP16 gas turbine rated at 1.9 MW [6]. Compared to the standard combustor used for burning fossil fuels in diffusion mode, the new design has a larger volume to provide enough residence time for complete burnout. The distribution of air was furthermore changed to ensure sufficient burning rates of the low-calorific fuels. Another major difference is the flame stabilization technique, which is now provided by a radial swirler only. Fuel is injected using a preforming airblast nozzle.

The simulations have been performed using a 45° section of the combustor to reduce the computational cost. Boundary conditions for the flow field and turbulence parameters imposed on the inlets of the domain were extracted from non-reacting flow simulations. The domain has been discretized using an unstructured tetrahedral grid with boundary layer elements. Local refinements were used to fill the width of a channel or hole with a minimum amount of 10 cells. The grid dependency study for the reacting flow domain included 9 different grids. In the finest grid, used as a reference, the global cell size was set to 2 mm. Comparison of the temperature and velocity profiles at various locations resulted in an optimized mesh containing 3.4 million cells, with local refinements near the atomizer, in the flame region and adjacent to the liner. Although considerably less elements were used compared to the 2 mm reference mesh, it was observed that velocity and temperature profiles at different sample lines along the combustor axis did not deviate more than 6%.

3.2. Gas phase modeling

The gas phase is described by the steady-state RANS equations. Favre-averaged conservation equations for mass, species, momentum and enthalpy have been solved to obtain the mean field quantities, while effects of turbulent fluctuations are modeled using the SST k - ω formulation as available in Fluent [50]. The density and heat capacity of the gas are computed from respectively the ideal gas law and a mixing law. Correlations for air are used to approximate the thermal conductivity and viscosity of the gas as function of temperature.

Radiative heat transfer has not been included in the model. This is a reasonable simplification for the low-soot ethanol flame, but may cause a more significant error in case of the pyrolysis oil flame. The luminosity of the latter has been observed to be roughly

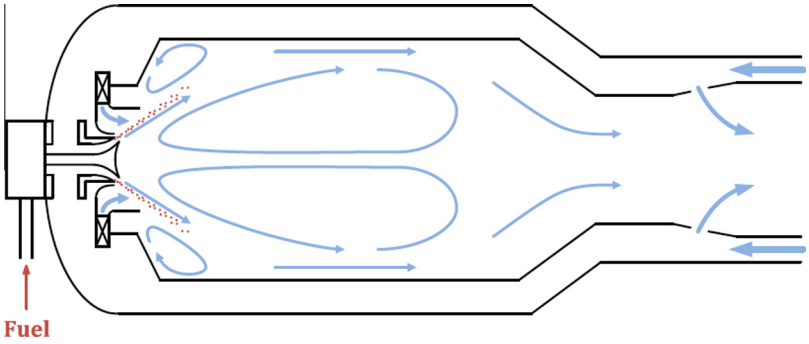

Fig. 1. Sketch of the biofuel combustor developed by OPRA Turbines [22]. The arrows indicate the flow field according to the current simulations.

in between that of ethanol and fuel oil [6,52]. The error on the droplet evaporation rate caused by neglecting radiation is acceptable since, for the small droplets considered here, convection is reported to be the dominant heat transfer mechanism [53].

3.3. Fuel spray definition

In the discrete phase model, the fuel spray is considered as a collection of parcels representing up to 75 droplets with the same properties. A transient solver tracks the parcels in a Lagrangian frame of reference while they exchange mass, heat and momentum with their surroundings. These processes are incorporated in the governing equations for each of the two phases by including source terms (two-way coupling). Since fuel sprays in gas turbines are typically characterized as dilute, any droplet-droplet interactions are unlikely to occur and can be neglected [54].

There is no experimental data available which describes the droplet size distribution produced by OPRA's prefilming airblast atomizer. Several empirical correlations for estimating the mean droplet size exist in the literature, but the predictions from these correlations show large differences. For the purpose of this study, it was therefore assumed that the droplets in the fuel sprays are uniform in size, i.e. 30 or 50 μm. Although such sprays are hypothetical and generally do not represent the real case, the uniformly-sized sprays give a clear indication of the relation between the flame and the drop size. Nevertheless, to illustrate the influence of the spread in the drop sizes observed in practical sprays, comparative simulations have been performed using a Rosin-Rammler distribution:

$$1 - F = e^{(D_d/\overline{D_d})^q} \tag{1}$$

where F is the volume fraction of the droplets with a diameter smaller than D_d. The distribution is defined by a characteristic diameter, $\overline{D_d}$, and a spread parameter, q. Following the approach described in Sallevelt et al. [51], the characteristic diameter was derived from an estimated Sauter mean diameter (SMD) using the correlation proposed by El-Shanawany and Lefebvre [55], while a typical value for the spread parameter was obtained from experimental data for water sprays [56]. For q = 3.45, this approach results in a distribution with a SMD of 42 μm and a $\overline{D_d}$ of 54 μm. Secondary breakup has been neglected because the Weber number is typically lower than 10, meaning that further breakup of the droplets may not occur [54].

3.4. Interphase transport

Once the parcels have been released, the parcel trajectories are computed from the drag force exerted by the flow. The drag coefficient for a parcel is approximated by that of a spherical particle. Other forces acting on the parcels, such as virtual mass and pressure gradient forces, are negligible compared to the aerodynamic drag. The effect of turbulent velocity fluctuations on the droplet trajectories has been taken into account using the discrete random walk model [50]. An approximate expression for the mass flux from the droplet surface is the Maxwell equation for the diffusion-based evaporation:

$$\dot{m}_d = -4\pi R_d D_v \rho (Y_{v,s} - Y_{v,\infty}) \tag{2}$$

where R_d is the droplet radius, D_v is the diffusion coefficient of the fuel vapor, ρ is the total density of the mixture in the vicinity of the droplet, and $Y_{v,s}$ and $Y_{v,\infty}$ are the fuel vapor mass fractions at the surface and in the far field. For the simulations with pyrolysis oil, Eq. (2) is solved for each fuel component listed in Table 1 and the total mass loss is the sum of the species mass fluxes. The physical and chemical properties of the individual species are taken into account as droplet evaporation proceeds.

Vapor concentrations at the droplet surface are computed from Raoult's law under the assumption of an ideal mixture in vapor-liquid equilibrium. The diffusion coefficients have been evaluated at a film-averaged temperature using the 1/3-rule recommended by Hubbard et al. [57]. For a spherical droplet in a static atmosphere, the Sherwood number in this model is equal to 2. To account for external convection around the droplet in the combustor, this value is corrected using the Ranz-Marshall correlation:

$$Sh = 2 + 0.6Re^{1/2}Sc^{1/3} \quad \text{and} \quad Nu = 2 + 0.6Re^{1/2}Pr^{1/3} \tag{3}$$

where Re, Sc and Pr are the Reynolds number, Schmidt number and Prandtl number, respectively.

Eq. (2) is generally valid for low evaporation rates since it ignores the convective flow of fuel vapor away from the droplet surface. The outward vapor flow induced at high evaporation rates is referred to as Stefan flow and impedes the transfer of mass and heat at the droplet surface.

A more general formulation for quasi-steady droplet evaporation that includes this effect has been developed in the 1950s [58,59]. Starting from the continuity equations for mass and species, it was derived that the evaporation rate can be described by Eq. (4), where B_M is the Spalding mass transfer number.

$$\dot{m}_d = -4\pi R_d D_v \rho \ln(1 + B_M) \quad \text{and} \quad B_M = (Y_{v,s} - Y_{v,\infty})/(1 - Y_{v,s}) \tag{4}$$

When assuming a Lewis number equal to unity, an equivalent expression for the rate of droplet mass loss can be obtained from the energy balance:

$$\dot{m}_d = \frac{-4\pi R_d k_g}{C_{p,v}} \ln(1 + B_T) \quad \text{and} \quad B_T = C_{p,v}(T_\infty - T_s)/L_{eff} \tag{5}$$

where k_g is the thermal conductivity of the gas, $C_{p,v}$ is the specific heat capacity of the vapor, B_T is the Spalding heat transfer number and L_{eff} is the effective latent heat of vaporization, defined as:

$$L_{eff} = L - (|\dot{q}_d|/\dot{m}_d) \tag{6}$$

where L is the specific latent heat and q_d is the conductive heat flux at the surface used to heat the droplet interior. By further evaluation it is found that the Sh and Nu numbers are now expressed by:

$$Sh = 2\frac{\ln(1+B_M)}{B_M} \quad \text{and} \quad Nu = 2\frac{\ln(1+B_T)}{B_T} \tag{7}$$

In the limit of low evaporation rates, $B_M \to 0$ and $B_T \to 0$ such that the solution for moving droplet, i.e. Eq. (3) is obtained. For droplets that are surrounded by a flame, the theory for a non-reacting atmosphere can be extended to obtain the burning rate of a drop in an oxidizing gas. The rate of mass loss of a burning droplet is given by Eq. (8) with a modified mass transfer number to account for the heat release near the drop surface:

$$B_{T,c} = \frac{C_{p,v}(T_\infty - T_s) + (Y_{O,\infty}/\sigma_O)q_c}{L_{eff}} \tag{8}$$

where the subscript c refers to combustion, qc is the heat of combustion and σ_O is the stoichiometric mass ratio of fuel and oxidizer.

When the droplet is in thermal equilibrium after an initial heat-up period, the square of the droplet diameter decreases linearly with time and is described by the well-known D^2-law, see Eq. (9). Note that the D^2-law does not hold for multicomponent fuels and is not used as assumption in the current model.

$$D_d^2(t) = D_{d,0}^2 - K \cdot t \tag{9}$$

where $D_{d,0}$ is the initial diameter of the droplet and K denotes the evaporation or burning rate constant. The linear trend has been confirmed by many experimental observations with single-component liquids. From the Maxwell equation the K value is given by:

$$K = \frac{8k_g}{\rho_l C_{p,v}}(Y_{v,s} - Y_{v,\infty}) \tag{10}$$

whereas from the Spalding the evaporation constants K_v and K_c are defined as:

$$K_v = \frac{8k_g}{\rho_l C_{p,v}} \ln\left(1 + \frac{C_{p,v}(T_\infty - T_s)}{L}\right) \quad \text{and}$$
$$K_c = \frac{8k_g}{\rho_l C_{p,v}} \ln\left(1 + \frac{C_{p,v}(T_\infty - T_s) + (Y_{O,\infty}/\sigma_O)q_c}{L}\right) \tag{11}$$

3.5. Liquid phase modeling

The selective evaporation of the various constituents of a multicomponent fuel can lead to significant mass and temperature gradients within the droplet. Consequently, the influence of internal transport on the evaporation process can be more pronounced than in case of pure liquids [60,61]. Simulation results are hence expected to be sensitive to the model used for describing the liquid phase transport mechanisms. However, solving transport equations inside each droplet requires large computational effort. The current CFD code therefore relies on the rapid mixing assumption, which is in line with the work of Hallett and Clark [18] and Zhang and Kong [21]. It is accordingly assumed that the droplet is spatially uniform in temperature and composition. The temperature change in time is computed from the global heat balance given by:

$$\dot{m}_d C_p \frac{dT_d}{dt} = 4\pi R_d^2 h(T_\infty - T_d) - \dot{m}_d L \tag{12}$$

where T_d is the droplet temperature, C_p is the droplet heat capacity and L is the latent heat of vaporization. Note that C_p and L are changing during the lifetime of the droplets in case of a multicomponent fuel. The heat transfer coefficient h is determined from the Nusselt number (Eq. (3)).

3.6. Combustion modeling

The pyrolysis oil flame is described by using a combustion model based on local equilibrium to allow for a changing composition of the fuel vapor. Under the assumption that species react toward their equilibrium state over a characteristic time, the mean local reaction rate for species i can be modeled as [50]:

$$R_i = \rho(Y_i^{eq} - Y_i)/\tau \tag{13}$$

where ρ is the mixture density, Y_i is the mean mass fraction as obtained from the species conservation equation, Y_i^{eq} is the local equilibrium mass fraction and τ denotes a characteristic time scale. The characteristic time is equated to the turbulent time-scale, which is described by the turbulence model:

$$\tau = \tau_{turb} = k/(A\epsilon) \tag{14}$$

where k is the turbulent kinetic energy, ε is the eddy dissipation rate and A is a model constant equal to 4 by default. This model will be referred to as the relaxation-to-equilibrium (RTE) model.

The RTE model has also been applied in the simulations with ethanol to facilitate comparisons with the pyrolysis oil cases. For modeling the ethanol flame, however, it is also feasible to use alternative models. The sensitivity of the temperature field to the chosen chemistry model is therefore evaluated by performing additional simulations with ethanol using the non-adiabatic steady laminar flamelet model, with temperature change but frozen species composition. The laminar ethanol flamelets were calculated on basis of a reaction mechanism developed by Röhl and Peters, including 38 species and 228 reactions [62]. The average temperature, density and species mass fractions in the turbulent flame were subsequently computed and stored in multidimensional look-up tables of the form:

$$\widetilde{\phi} = \widetilde{\phi}(\widetilde{Z}, \widetilde{Z''^2}, \widetilde{\chi_{st}}, \widetilde{H}) \tag{15}$$

where $\widetilde{\phi}$ is the quantity of interest, $\widetilde{Z}$ is the mean mixture fraction, $\widetilde{Z''^2}$ is the mixture fraction variance, $\widetilde{\chi_{st}}$ is the stoichiometric scalar dissipation rate, and $\widetilde{H}$ is the mean enthalpy level.

3.7. Boundary conditions and case specification

Air enters the domain with a total flow rate of 300 g/s at a temperature equal to the compressor discharge temperature in OPRA's OP16 engine. The thermal input is set to 280 kW in all simulations, which corresponds to a fuel flow rate of 10.5 g/s for ethanol and 17.9 g/s for pyrolysis oil. A pressure condition is applied at the outlet. The combustor walls are assumed to be adiabatic. Impingement of droplets on the liner is described by the wall-jet boundary condition [50]. The wall-jet model predicts the trajectory of a droplet after impacting a high-temperature wall where no liquid film is formed. The droplet size distribution and the combustion model have been varied to study the influence of these settings on the solution. Table 3 gives an overview of the settings used in the reacting flow simulations. A more detailed description of these models can be found in Sections 3.3 and 3.6.

3.8. Solution method

The system of equations was solved using a pressure-based AMG solver with a pressure-velocity coupling algorithm. Values on the cell faces were computed using the second-order upwind scheme. Explicit as well as implicit under-relaxation was used to

Table 3
Overview of the models used for the reacting flow simulations.

Case	Fuel	Combustion model	Droplet size and distribution
E.1	Ethanol	RTE	Uniform, 50 μm
E.2	Ethanol	RTE	Rosin-Rammler
E.3	Ethanol	RTE	Uniform, 30 μm
E.4	Ethanol	Flamelets	Uniform, 50 μm
PO.1	Pyrolysis oil	RTE	Uniform, 50 μm
PO.2	Pyrolysis oil	RTE	Rosin-Rammler
PO.3	Pyrolysis oil	RTE	Uniform, 30 μm

stabilize the solver. The PRESTO! Scheme has been selected for the pressure interpolations.

4. Results and discussion

The results for ethanol and pyrolysis oil combustion using the same model configuration are discussed first. Subsequently, it is examined to what extent the solution is sensitive to the droplet size and the combustion model. Temperatures and velocities have been made dimensionless through division of the values by a constant reference value. The overall mass and heat imbalance were respectively below 0.01% of the total mass flow rate and below 0.3% of the heat of combustion (280 kW ± 0.5%). Whenever possible, the numerical data are validated with experiments performed by OPRA with the same combustor configuration [6]. The predicted air distribution over the combustor zones agrees well with the measurements, with an error of less than 1% of the total flow.

4.1. Maxwell vs Spalding evaporation

To investigate the sensitivity of the droplet life to the evaporation model, additional simulations have been performed with the Spalding (Eq. (4)) and Maxwell (Eq. (2)) evaporation model. A quantitative evaluation of the difference in vaporization rate is given in Fig. 2 for E.1 ethanol case. Figure shows that the evaporation rate constant predicted by the Spalding model is only 0.54 mm^2/s, which results in a 65% increase in average droplet lifetime. Such long evaporation times are highly unlikely considering the measured regression rates listed in Table 4. This indicates that the droplet should be regarded as burning rather than evaporating when using the Spalding theory under these conditions. In other words, more accurate results can be expected from the droplet combustion model given by Eq. (5) combined with Eq. (8). Calculations performed by Shaddix and Hardesty [63] show that the burning rate predicted by Eq. (11) is typically 1.5–2.0 times higher than the evaporation rate for diesel and pyrolysis oil droplets. This ratio between K_c and K_v agrees well with the difference between the measured and predicted surface regression rates for ethanol as observed in this study.

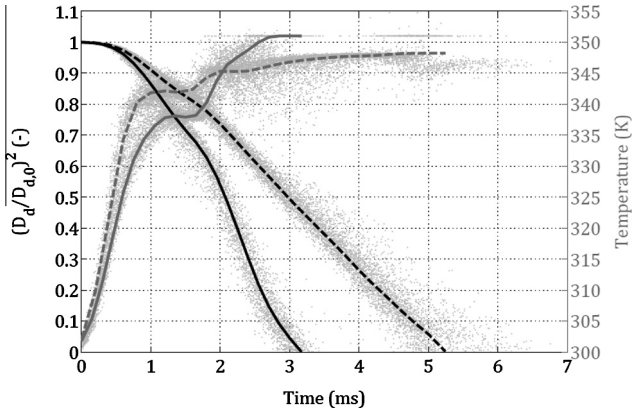

Fig. 2. Comparison of the square of the non-dimensional droplet diameter and the droplet temperature of ethanol combustion as function of time, computed using the Maxwell (solid) and the Spalding evaporation model (dashed).

From the models considered in the present simulations, the Maxwell equation is thus observed to give the most credible results (see also discussion in Section 4.2). A possible explanation is that the adverse effect of Stefan convection at the drop surface is compensated by the flame surrounding the droplet. The oversimplified Maxwell equation, in which both these effects are not included, may therefore still be capable of providing reasonable estimations for the droplet lifetime.

4.2. Temperature field and evaporation behavior

Fig. 3(left) shows the temperature contours for ethanol (Case E.1) in the top half and for pyrolysis oil (Case PO.1) in the bottom half, together with the corresponding fuel sprays. In these simulations, the chemistry is predicted by using the RTE model, and droplets are 50 μm in diameter (see Table 3). The peak temperatures for the ethanol case are reached near the atomizer pintle and near the combustor axis further downstream. The temperatures in these regions are in close agreement with the adiabatic flame temperature. In the pyrolysis oil case, the peak temperature is observed close to the liner and is only 2140 K. This temperature is significantly lower than the adiabatic flame temperature of 2287 K for the pyrolysis oil surrogate fuel. However, it is very well possible that the maximum temperature of the pyrolysis oil flame does not correspond to the adiabatic value because the fuel components are not released simultaneously (see Fig. 4). The differences in molecular formulas of the vaporizing components make that a wide range of local C–H–O ratios are possible. In practice, the flame temperatures for both fuels are expected to be slightly lower than predicted by the model, primarily since radiative heat losses are neglected.

The total amount of energy required for evaporating the fuel is more than twice as high for pyrolysis oil as for ethanol, i.e. 20.5 kW compared to 9.5 kW. As illustrated by Fig. 3(left), the evaporating pyrolysis oil droplets therefore cause a large decrease in gas temperature near the spray. Since the majority of the combustion heat is released during the latter half of the droplet lifetime, after the water has evaporated, ignition and combustion in the proximity of the atomizer will proceed at a lower rate. During experiments

Table 4
Comparison of evaporation constants for vaporizing or burning ethanol droplets. Temperatures and velocities from the simulations are typical values.

Author(s)	Method	$D_{d,0}$ (μm)	T_{gas} (K)	U_{rel} (m/s)	K (mm^2/s)
Godsave [58]	Exp.	1500	T_{flame}	Quiescent	0.81
Goldsmith [64]	Exp.	1500–1800	T_{flame}	Quiescent	0.86
Maqua et al. [65]	Exp.	105	1140	5–6	0.81
			1260	4–5	0.71
			1270	2–4	0.73
Current	Num. (Maxwell model)	50	800–1800	5–20	0.98

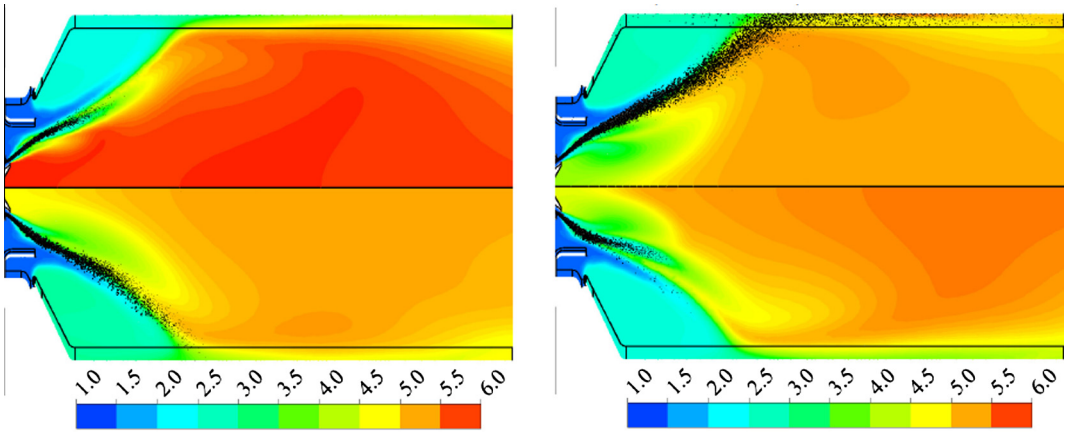

Fig. 3. Comparison of the temperature fields and fuel sprays. Left: ethanol (top) and pyrolysis oil (bottom) combustion (Case E.1 vs PO.1) and right: pyrolysis oil combustion using a Rosin-Rammler distribution (top) and using a uniform drop size of 30 μm (bottom) (Case PO.2 vs PO.3).

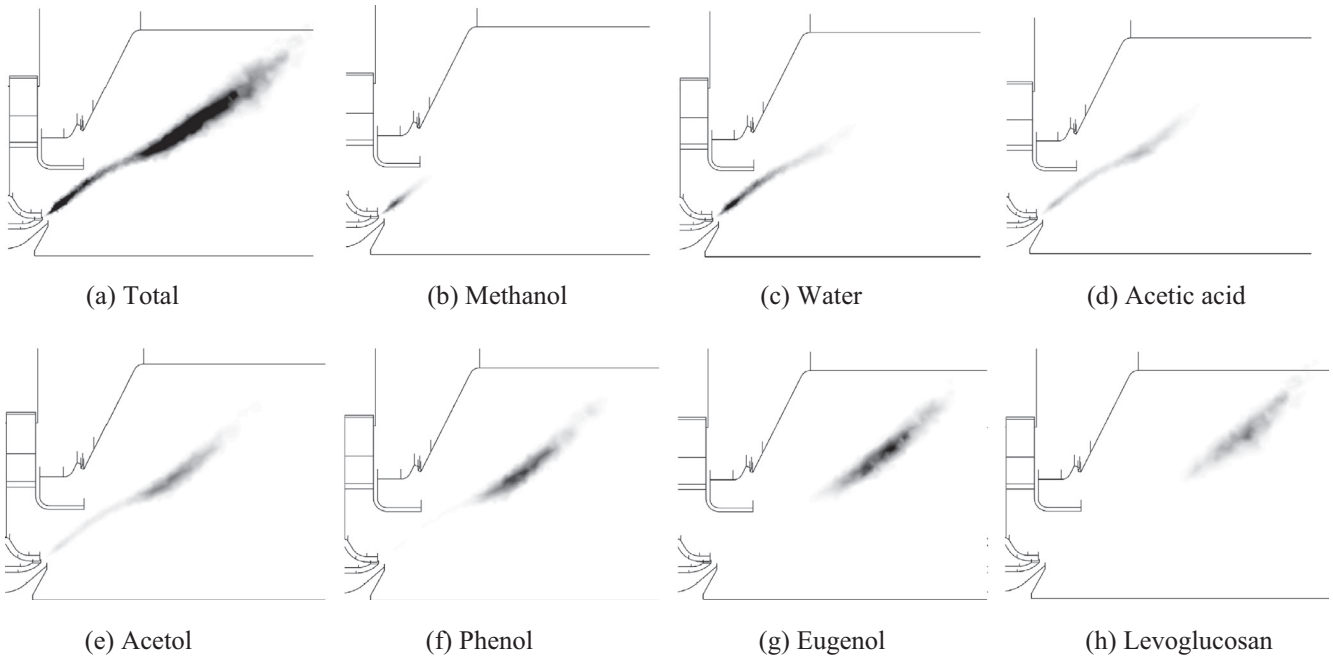

Fig. 4. Rate of mass transfer to the gas phase for the total droplet (a) and for each individual component (b–h) in the pyrolysis oil surrogate, using the same intensity scaling. The plots give qualitative insight into the vaporization regions of the components in case of a uniform droplet size of 50 μm (Case PO.1).

with pyrolysis oil in OPRA's atmospheric test rig [6], this effect has been reported as a decreased flame stability.

It is also observed that the pyrolysis oil spray penetrates considerably further into the combustor. A qualitative impression of the subsequent evaporation of fuel species can be found in Fig. 4. To get detailed insight into the evaporation process, Fig. 5 reports the square of the non-dimensional diameter and the temperature of the droplets in the ethanol and pyrolysis oil spray as function of time. The small dots indicating the current state of each droplet show a significant degree of scattering due to the modeled effect of turbulent velocity fluctuations (see Section 3.4). For the sake of convenience, this discussion will only consider averaged values at each point of time, which are indicated by the solid curves for ethanol and the dashed curves for pyrolysis oil.

The figure shows that the evaporation curve for ethanol approximates the D^2-law given by Eq. (9). After a short heat-up period the temperature tends to stabilize between 338 and 351 K, whereby the exact value varies with the conditions of the droplet surroundings. The evaporation rate constant in Eq. (9) can be determined from the average slope of the diameter curve from this point ($t \geqslant 1$ ms) and is found to be 0.98 mm^2/s. In Table 4, this result is compared to experimental values reported in the literature for vaporizing or burning ethanol droplets. The somewhat higher value found in this work is probably related to the velocity of the droplets relative to the gas, U_{rel}, which is generally much higher in the current simulations. According to the correlation that accounts for the effects of gas phase convection on the evaporation rate, Eq. (3), the external velocity can have major impact on the vaporization rate via the Reynolds number. Nevertheless, since measured values for higher velocities or typical Re numbers have not been found in the literature, the accuracy of the predicted evaporation curve for these conditions cannot be fully confirmed.

The dashed curves in Fig. 5 show the evaporation of the multi-component pyrolysis oil surrogate. A rapid increase in temperature is again observed within the first millisecond, where already part of the methanol escapes from the drop surface. The temperature

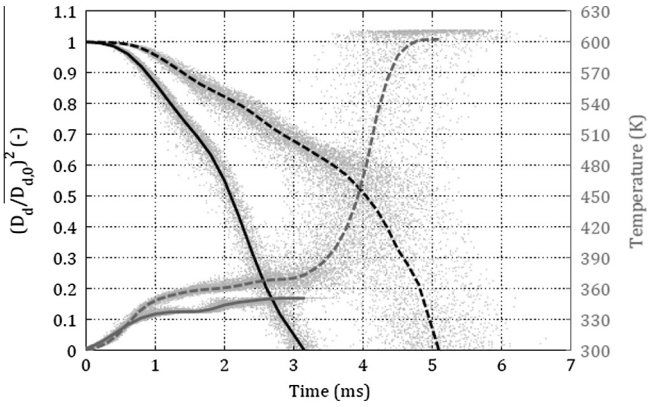

Fig. 5. Comparison of the square of the non-dimensional droplet diameter and the droplet temperature as function of time for the ethanol (solid) and pyrolysis oil (dashed) spray (Cases E.1 and PO.1).

curve then levels off while the remaining methanol, the water and part of the acetic acid vaporize. The D^2-curve shows that the evaporation rate constant is only 0.36 mm^2/s at this stage, which is largely due to the high latent heat of the water. This adds to the effect of the relatively high density of the surrogate fuel, increasing from 1050 kg/m^3 to 1317 kg/m^3 over the droplet lifetime.

When practically all the water has been released around t = 3.5 ms, the temperature curve steeply increases up to the final value just above 600 K, where the levoglucosan evaporates in an equilibrium state. The heating rate in this latter part of the curve is an important indicator for the formation of char inside the droplet. From this model, it follows that the mean heating rate is $8 \cdot 10^6$ K/min. This result suggests a low tendency of the droplets to form solid residue according to earlier studies (see Section 2). During combustion tests with pyrolysis oil using airblast atomization, sparks were indeed hardly observed in the flue gases. The average evaporation rate constant after t = 3.5 ms is changing to 1.0 mm^2/s. In this time range, however, the evaporation rate is also influenced by the significant increase in temperature of the surrounding gas. Whereas the droplet surrounding is typically around 1000 K up to this point, temperatures up to 2000 K are reached at the end of the curve.

Experimental data to validate the pyrolysis oil results are hardly available, but some valuable measurements have been performed by Shaddix and Hardesty [63]. For poplar and switchgrass oil droplets with an initial diameter of 350 μm, they found that the burning rate "ranged from ≈ 0.3 mm^2/s (shortly after the droplet heat-up period) to 0.5–0.6 mm^2/s at later residence times". An important note is that the square of the non-dimensional droplet diameter in these measurements did not reach values lower than 0.75 and 0.85 for respectively the poplar and switchgrass oil due to the occurrence of micro-explosions. Nevertheless, these data suggest that the model predicts a representative surface regression rate for the first part of the evaporation curve. The total lifetime of a pyrolysis oil droplet is roughly 60% longer than that of an ethanol droplet. If compared to the evaporation time for diesel No. 2, even larger differences can be expected since reported burning rates for diesel are slightly higher than for ethanol under similar conditions [58,63]. This outcome underlines the need for large combustion chambers and fine atomization for burning pyrolysis oil successfully.

4.3. Influence of the initial droplet size

As explained in Section 3.3, the uniform droplet size used in this study does not reflect the diameter variations observed in practical fuel sprays. The possible influence of this simplification on the results has been examined by performing an additional simulation with ethanol and pyrolysis oil, in which the uniform size was replaced by a Rosin-Rammler distribution defined in Section 3.3. This section also discusses the results for a uniform droplet size of 30 μm instead of 50 μm, simulating extremely fine atomization.

The simulations for ethanol using a droplet size distribution (Case E.2) shows that the spray reaches much further into the domain as it contains larger droplets. However, aside from the difference in spray penetration, the temperature and velocity fields are very similar to those for the uniform 50 and 30 μm droplet size cases (E.1 and E.3). The results for ethanol combustion are hence found to be remarkably insensitive to the exact size distribution of the droplets specified at the injection location.

In case of pyrolysis oil combustion, the influence of the droplet size on the temperature field is more pronounced. This is illustrated by Fig. 3(right), which compares the results for a non-uniform drop size (top) to those for a uniform size of 30 μm (bottom) (Case PO.2 vs PO.3). For both cases, the temperature field is significantly different with respect to the base case with a uniform size of 50 μm, shown in the bottom half of Fig. 3(left). An important difference with ethanol is that most of the energy in this fuel is released after the evaporation of the water. When using the Rosin-Rammler distribution (Case PO.2) instead of a uniform size of 50 μm (Case PO.1), a significant part of the fuel reaches this stage in the evaporation process relatively soon due to the presence of small droplets in the spray. This causes the flame temperature to rise faster in the first case. On the other hand, the largest droplets in the distribution do not fully evaporate before impacting the combustor liner. A small fraction of the fuel is therefore burning along the liner wall, where it forms a thin, hot film of product gases.

Impingement of drops on the liner is found to occur for initial diameters larger than 65 μm. This diameter should hence be considered as the maximum desirable droplet size to avoid possible coke formation on the inner liner walls. However, since droplet diameters up to 100 μm are common in practical fuel sprays, it is likely that the spray is partly impacting the liner. This scenario

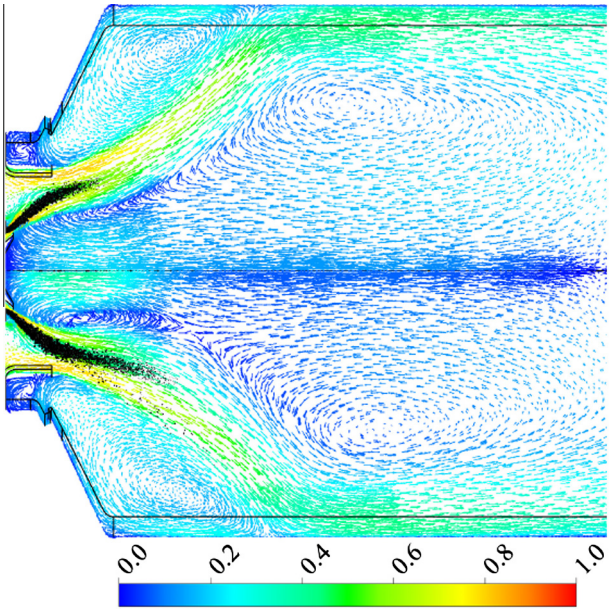

Fig. 6. Comparison of the velocity fields for ethanol (top) and pyrolysis oil (bottom) combustion using a uniform drop size of 30 μm (Case E.3 vs PO.3). An additional circulation region is formed in case of pyrolysis oil. The colors are based on the velocity magnitude. (For interpretation of the references to color in this figure legend, the reader is referred to the web version of this article.)

Table 5
Predicted and measured CO_2 emissions and outlet temperatures. The model predictions in this table are flow-averaged values in the dry gas. Experimental values have been provided by OPRA. The temperatures are non-dimensional and the concentrations have been normalized to 15% oxygen.

Case	CO_2 (%)	T_{out} (–)	Case	CO_2 (%)	T_{out} (–)
E.1	4.27	3.21	PO.1	5.34	3.16
E.2	4.27	3.21	PO.2	5.34	3.15
E.3	4.27	3.21	PO.3	5.32	3.15
E.4	4.19	3.17			
Exp.	4.27	2.79	Exp.	5.45	2.86

has been confirmed by test runs with pyrolysis oil, after which some droplet traces were observed on the liner wall around the impact location. Furthermore, it explains why the removal of film cooling on the liner inner wall resulted in a considerable decrease of sediments in preliminary tests with the down-scaled standard combustor [6,16]. At engine conditions, however, spray impingement is hardly expected to occur because the atomization quality is known to improve at higher pressures.

Changing the droplet size in the pyrolysis oil cases not only influences the temperature field, but also affects the flow field close to the atomizer. When either using a size distribution (Case PO.2) or a very fine spray (PO.3), an additional circulation region is formed in front of the nozzle pintle. It is remarkable, however, that the flow pattern remains unchanged when varying the droplet size in the simulations with ethanol. Fig. 6 compares the flow fields and sprays of the ethanol and pyrolysis oil simulations using 30 μm as the drop size (Case E.3 vs PO.3). The top half of the figure represents the ethanol case and shows the strong curvature in the flow near the pintle as seen in most of the simulations. In the bottom half, it can be seen that the curvature has turned into a separate vortex. The temperature in this zone is significantly lower compared to the previous situation (typically by 150–300 K), since the new circulation contains part of the atomizing air that otherwise would have followed the swirler air in outward direction. The vortex can thus have adverse consequences for the evaporation and ignition of the fuel, and might affect the performance of the combustor in practice.

The temperature field in the 30 μm pyrolysis oil case is further influenced by the altered spray path as seen in the bottom half of Fig. 6. The small droplets are carried in a more forward direction compared to the path of the 50 μm shown in Fig. 3(left), such that the fuel is largely located at the inner side of the bulk flow originating from the nozzle and the swirler. This reduces the mixing of hot product gases on the outer side and therefore results in a lower temperature in the circulation region adjacent to the dome. In combination with the relatively cold vortex in front of the nozzle, the temperature on both sides of the spray has become lower and the combustion heat is more concentrated in the core region of the burner at some distance from the nozzle (see Fig. 3).

4.4. Comparison of the combustion models

The flame characteristics for the multicomponent pyrolysis oil were calculated by employing the RTE model, in which the gas phase reacts towards local equilibrium with a finite reaction rate (see Section 3.6). In case of ethanol, simulations were performed also with the flamelet model instead of the RTE model in order to incorporate effects of turbulence and flame strain. The flamelet model has shown already a good agreement with experimental data in the former study, see [51]. The results obtained with the RTE model on the one hand, and the flamelet model on the other hand, have been compared for this fuel (Case E.1 vs E.4) on basis of the CO_2 mole fraction. From this comparison, it can be concluded that the overall reaction towards CO_2 proceeds slower in case of the flamelet model. As a consequence, this model predicts a more distributed release of combustion heat over the combustor volume. Aside from this difference, however, the RTE model provides a similar temperature field as the flamelet model. This suggests that the RTE model may also be used to obtain adequate predictions for the pyrolysis oil flame as long as detailed combustion kinetics are not available. For more advanced models that may be applicable in this case, the authors refer to a review by Jenny et al. [66].

4.5. Temperatures and CO_2 emissions

The CO_2 concentrations and dimensionless temperatures at the outlet are given in Table 5. The table includes predictions from the CFD model as well as experimental data obtained by OPRA at similar operating conditions [6]. The normalized CO_2 concentrations correspond to the theoretical values based on the atomic ratios of the two fuels and are in good agreement with the measured values. This is an important validation of the overall credibility of the model. Regarding the temperatures, however, the measured values are considerably lower than predicted by the model due to the non-uniform temperature profile at the outlet. Similar deviations have been observed in [51], where CFD results were compared to experiments in OPRA's conventional fuel burner and adiabatic temperature calculations.

The table furthermore shows that, for the same model configuration, the predicted outlet temperature for pyrolysis oil combustion is slightly lower compared to the ethanol case (Cases PO.1 and E.1). This temperature difference is mainly caused by the higher total mass flow rate in the first case. The lower temperature and CO_2 concentration reported for Case E.4 is due to the high CO level predicted by the flamelet model used in this simulation. The presence and location of the recirculation zone inside the combustor was confirmed in the experiments on the basis of droplet markings on the liner. Furthermore the air split in the combustor corresponded very well with experimental data (obtained in cold flow conditions).

5. Conclusions

The combustion of ethanol and fast pyrolysis oil in OPRA's low-calorific fuel burner has been modeled using the Euler Lagrange RANS method in ANSYS Fluent. Given the complex, multicomponent nature of pyrolysis oil, a surrogate fuel has been developed to obtain a feasible implementation of its properties in the CFD code. Comparing the results obtained for pyrolysis oil and ethanol burning, it is found that the peak combustion temperature is relatively low in the pyrolysis oil case. The difference cannot be fully explained by the lower adiabatic flame temperature of pyrolysis oil, and could, therefore, be related to the multicomponent evaporation and mixing. The pyrolysis oil surrogate requires twice as much evaporation heat compared to ethanol, resulting in a decreased flame stability. The total lifetime of a 50 μm pyrolysis oil droplet is approximately 60% longer than that of an ethanol droplet of the same size. For this particular combustor, pyrolysis oil droplets larger than 65 μm are seen to impinge on the combustor

liner. These findings underline the importance of a large primary zone and of fine atomization for the combustion of pyrolysis oil. The numerical results for the pyrolysis oil behavior in gas turbines are in agreement with the experimental data available, but further research is needed to validate the simulations in more detail.

Regarding the spray modeling, it is seen that results for ethanol are remarkably insensitive to the initial droplet size defined at the injection location. In case of pyrolysis oil, however, changing the droplet size leads to differences in both the temperature and the velocity field. The ethanol flame has been predicted using two different combustion models. Comparative simulations have shown that a model based on a local balance between diffusion and reaction gives similar predictions as the flamelet model. This suggests that, except for pollutant emissions, the first approach can be used to predict a pyrolysis oil flame with fair accuracy.

Acknowledgements

This work is part of the BE2.O program, funded by the Province of Overijssel. The authors thank Riza Yukananto for his contributions to the preliminary modeling, and Mr. Martin Beran and Dr. Lars-Uno Axelsson from OPRA Turbines for their collaboration during this project.

References

[1] Krumdieck SP, Daily JW. Evaluating the feasibility of biomass pyrolysis oil for spray combustion applications. Combust Sci Technol 1998;134(1–6):351–65. http://dx.doi.org/10.1080/00102209808924140.
[2] Czernik S, Bridgwater AV. Overview of applications of biomass fast pyrolysis oil. Energy Fuels 2004;18(2):590–8. http://dx.doi.org/10.1021/ef034067u. ISSN 0887-0624.
[3] Lupandin V, Thamburaj R, Nikolayev A. Test results of the OGT2500 gas turbine engine running on alternative fuels: biooil, ethanol, biodiesel and crude oil. In: ASME turbo expo 2005, ASME, Reno, NV, USA. p. 421–6. http://dx.doi.org/10.1115/GT2005-68488.
[4] Chiaramonti D, Oasmaa A, Solantausta Y. Power generation using fast pyrolysis liquids from biomass. Renew Sustain Energy Rev 2007;11(6):1056–86. http://dx.doi.org/10.1016/j.rser.2005.07.008. ISSN 13640321.
[5] Gupta KK, Rehman A, Sarviya RM. Bio-fuels for the gas turbine: a review. Renew Sustain Energy Rev 2010;14(9):2946–55. http://dx.doi.org/10.1016/j.rser.2010.07.025.
[6] Beran M, Axelsson L-U. Development and experimental investigation of a tubular combustor for pyrolysis oil burning. J Eng Gas Turbines Power 2015;137(3):31508. http://dx.doi.org/10.1115/1.4028450.
[7] Lujaji FC, Boateng AA, Schaffer MA, Mullen CA, Mkilaha ISN, Mtui PL. Pyrolysis oil combustion in a horizontal box furnace with an externally mixed nozzle. Energy Fuels 2016;30:4126–36. http://dx.doi.org/10.1021/acs.energyfuels.6b00318.
[8] Van de Beld B, Holle E, Florijn J. The use of pyrolysis oil and pyrolysis oil derived fuels in diesel engines for CHP applications. Appl Energy 2013;102:190–7.
[9] Sallevelt JLHP, Gudde JEP, Pozarlik AK, Brem G. The impact of spray quality on the combustion of a viscous biofuel in a micro gas turbine. Appl Energy 2014;132:575–85.
[10] Ji-Lu Z, Yong-Ping K. Spray combustion properties of fast pyrolysis bio-oil produced from rice husk. Energy Convers Manage 2010;51:182–8.
[11] Jayaraman K, Gökalp I. Pyrolysis, combustion and gasification characteristics of miscanthus and sewage sludge. Energy Convers Manage 2015;89:83–91.
[12] Lehto J, Oasmaa A, Solantausta Y, Kytö M, Chiaramonti D. Review of fuel oil quality and combustion of fast pyrolysis bio-oils from lignocellulosic biomass. Appl Energy 2014;116:178–90.
[13] Sallevelt JLHP, Pozarlik AK, Brem G. Characterization of viscous biofuel sprays using digital imaging in the near field region. Appl Energy 2015;147:161–75.
[14] Strenziok R, Hansen U, Kunstner H. Combustion of bio-oil in a gas turbine. In: Bridgwater AV, editor. Progress in thermochemical biomass conversion. Oxford, UK: Blackwell Science Ltd; 2001. p. 1452–8. http://dx.doi.org/10.1002/9780470694954.ch119 [chapter 119].
[15] Pozarlik AK, Bijl A, Van Alst N, Pander R, Bramer EA, Brem G. Combustion of pyrolysis oil blends with diesel fuel in a micro gas turbine. In: Proceedings of EUBCE 2016, 24 European biomass conference & exhibition, 6–9.06.2016, Amsterdam, The Netherlands.
[16] Beran M. Pyrolysis oil application in OPRA gas turbines. URL <http://www.bioliquids-chp.eu/news.php?aid=16> [accessed 2016-02-03].
[17] Lederlin T. A model of bio-oil evaporation for Master thesis. Carleton University; 2002.
[18] Hallett WLH, Clark NA. A model for the evaporation of biomass pyrolysis oil droplets. Fuel 2006;85(4):532–44. http://dx.doi.org/10.1016/j.fuel.2005.08.006.
[19] Brett J, Ooi A, Soria J. The effect of internal diffusion on an evaporating bio-oil droplet – the chemistry free case. Biomass Bioenergy 2010;34(8):1134–40. http://dx.doi.org/10.1016/j.biombioe.2010.03.006.
[20] McGrath AT. Development of a computational fluid dynamics model for combustion of fast pyrolysis liquid (bio-oil) Master thesis. University of Toronto; 2011.
[21] Zhang L, Kong SC. Multicomponent vaporization modeling of bio-oil and its mixtures with other fuels. Fuel 2012;95:471–80. http://dx.doi.org/10.1016/j.fuel.2011.12.009.
[22] Beran M, Koranek M, Axelsson L-U. United States Patent Application for low calorific fuel combustor for gas turbines, no. 12/926,321; 2010.
[23] Branca C, Di Blasi C, Elefante R. Devolatilization and heterogeneous combustion of wood fast pyrolysis oils. Ind Eng Chem Res 2005;44(4):799–810. http://dx.doi.org/10.1016/j.tca.2005.02.030.
[24] Branca C, Di Blasi C. Multistep mechanism for the devolatilization of biomass fast pyrolysis oils. Ind Eng Chem Res 2006;45(17):5891–9. http://dx.doi.org/10.1021/ie060161x.
[25] Gómez MA, Porteiro J, Patiño D, Míguez JL. Eulerian CFD modelling for biomass combustion. Transient simulation of an underfeed pellet boiler. Energy Convers Manage 2015;101:666–80.
[26] Scherer V, Mönnigmann M, Berner MO, Sudbrock F. Coupled DEM–CFD simulation of drying wood chips in a rotary drum – baffle design and model reduction. Fuel 2016;184:896–904.
[27] Gómez MA, Porteiro J, de la Cuesta D, Patiño D, Míguez JL. Numerical simulation of the combustion process of a pellet-drop-feed boiler. Fuel 2016;184:987–99.
[28] Wang M, Liao B, Liu Y, Wang S, Qing S, Zhang A. Numerical simulation of oxy-coal combustion in a rotary cement kiln. Appl Therm Eng 2016;103:491–500.
[29] Oasmaa A, Solantausta Y, Arpiainen V, Kuoppala E, Sipila K. Fast pyrolysis bio-oils from wood and agricultural residues. Energy Fuels 2009;24(2):1380–8. http://dx.doi.org/10.1021/ef901107f.
[30] Van Rossum G, Guell BM, Ramachandran RPB, Seshan KS, Lefferts L, Van Swaaij WPM, et al. Evaporation of pyrolysis oil: product distribution and residue char analysis. AIChE J 2010;56(8):2200–10. http://dx.doi.org/10.1002/Aic.12126.
[31] Chhiti Y, Salvador S, Commandre JM, Broust F. Thermal decomposition of bio-oil: focus on the products yields under different pyrolysis conditions. Fuel 2012;102:274–81. http://dx.doi.org/10.1016/j.fuel.2012.06.098. ISSN 0016-2361.
[32] Branca C, Giudicianni P, Di Blasi C. GC/MS characterization of liquids generated from low-temperature pyrolysis of wood. Ind Eng Chem Res 2003;42(14):3190–202. http://dx.doi.org/10.1021/ie030066d.
[33] Tzanetakis T, Farra N, Moloodi S, Lamont W, McGrath A, Thomson MJ. Spray combustion characteristics and gaseous emissions of a wood derived fast pyrolysis liquid-ethanol blend in a pilot stabilized swirl burner. Energy Fuels 2010;24(10):5331–48. http://dx.doi.org/10.1021/Ef100670z.
[34] Oasmaa A, Kuoppala E, Solantausta Y. Fast pyrolysis of forestry residue. 2. Physicochemical composition of product liquid. Energy Fuels 2003;17(2):433–43. http://dx.doi.org/10.1021/ef901107f.
[35] Lehto J, Oasmaa A, Solantausta Y, Kyto M, Chiaramonti D. Fuel oil quality and combustion of fast pyrolysis bio-oils. VTT Technol 2013;87:79.
[36] Linstrom PJ, Mallard WG, editors. NIST chemistry webbook, NIST standard reference database number 69. Gaithersburg, MD: National Institute of Standards and Technology; 2014. URLAvailable from: <http://webbook.nist.gov>.
[37] Goos E, Burcat A, Ruscic B. Extended third millennium ideal gas and condensed phase thermochemical database for combustion with updates from active thermochemical tables URLAvailable from: <http://burcat.technion.ac.il/dir/>2010.
[38] Goos E, Burcat A, Ruscic B. New NASA thermodynamic polynomials database with active thermochemical tables updates. Report ANL 05/20 TAE 960 URLAvailable from: <http://burcat.technion.ac.il/dir>2014.
[39] CRECK Modeling Group. POLIMI BIO1212 thermodynamic database; 2012.
[40] Green DW et al. Perry's chemical engineers' handbook, 8th ed., vol. 796. New York: McGraw-Hill; 2008. http://dx.doi.org/10.1036/0071422943. ISBN 9780071422949.
[41] Dean JA, Lange NA. Lange's chemistry handbook, vol. 4. McGraw-Hill, Inc; 1999. p. 1424.
[42] Lide DR, editor. CRC handbook of chemistry and physics, internet version 2005. Boca Raton, FL: CRC Press; 2005. URLAvailable from: <www.hbcpnetbase.com>.
[43] Coker AK. Ludwig's applied process design for chemical and petrochemical plants. Ludwig's applied process design for chemical and petrochemical plants, 4th ed., vol. 1. Elsevier Science; 2007. ISBN 9780750677660.
[44] Wiley Information Services GmbH. Infotherm – database of thermophysical properties; 2014. URL <http://www.infotherm.com/>.
[45] Suuberg EM, Oja V. Vapor pressures and heats of vaporization of primary coal tars. Tech rep. Federal Energy Technology Center; 1997. http://dx.doi.org/10.2172/774960.
[46] Rihani DN, Doraiswamy LK. Estimation of heat capacity of organic compounds from group contributions. Ind Eng Chem Fundam 1965;4(1):17–21. http://dx.doi.org/10.1021/i160013a003.
[47] Reid RC, Prausnitz JM, Poling BE. The properties of liquids and gases. New York: McGraw-Hill; 1987.

[48] Baum E. Chemical property estimation: theory and application. CRC Press; 1997. ISBN 9780873719384.
[49] Acree Jr W, Chickos JS. Phase transition enthalpy measurements of organic and organometallic compounds. Sublimation, vaporization and fusion enthalpies from 1880 to 2010. J Phys Chem Ref Data 2010;39(4):43101. http://dx.doi.org/10.1063/1.3309507.
[50] Ansys. Ansys fluent theory guide, release 14.5; 2012.
[51] Sallevelt JLHP, Pozarlik AK, Beran M, Axelsson L-U, Brem G. Bioethanol combustion in an industrial gas turbine combustor: simulations and experiments. J Eng Gas Turb Power 2014;136(7). http://dx.doi.org/10.1115/1.4026529.
[52] Wissmiller D, Brown RC, Meyer TR. Pyrolysis oil combustion characteristics and exhaust emissions in a swirl-stabilized flame PhD thesis. Iowa State University; 2009.
[53] Tseng CC, Viskanta R. Effect of radiation absorption on fuel droplet evaporation. Combust Sci Technol 2005;177(8):1511–42. http://dx.doi.org/10.1080/00102200590956696.
[54] Faeth GM, Hsiang L-P, Wu P-K. Structure and breakup properties of sprays. Int J Multiph Flow 1995;21:99–127. http://dx.doi.org/10.1016/0301-9322(95)00059-7. ISSN 03019322.
[55] El-Shanawany MS, Lefebvre AH. Airblast atomization: effect of linear scale on mean drop size. J Energy 1980;4(4):184–9.
[56] Lefebvre AH. Atomization and sprays. CRC; 1988.
[57] Hubbard GL, Denny VE, Mills AF. Droplet evaporation: effects of transients and variable properties. Int J Heat Mass Transfer 1975;18(9):1003–8. http://dx.doi.org/10.1016/0017-9310(75)90217-3.
[58] Godsave GAE. Studies of the combustion of drops in a fuel spray – the burning of single drops of fuel. Symposium (international) on combustion, vol. 4. Elsevier; 1953. p. 818–30. http://dx.doi.org/10.1016/S0082-0784(53)80107-4.
[59] Spalding DB. Some fundamentals of combustion, vol. 2. Academic Press; 1955.
[60] Sirignano WA. Fluid dynamics and transport of droplets and sprays. 2nd ed. Cambridge University Press; 2010. ISBN 9780521884891.
[61] Abdel-Qader Z, Hallett WLH. The role of liquid mixing in evaporation of complex multicomponent mixtures: modelling using continuous thermodynamics. Chem Eng Sci 2005;60(6):1629–40. http://dx.doi.org/10.1016/j.ces.2004.10.015.
[62] Rohl O, Peters N. A reduced mechanism for ethanol oxidation. In: 4th European combustion meeting, Vienna, Austria, 14–17, 2009.
[63] Shaddix CR, Hardesty DR. Combustion properties of biomass flash pyrolysis oils: final project report. Tech rep SAND99-8238. Livermore, CA, USA: Sandia National Labs.; 1999.
[64] Goldsmith M. The burning of single drops of fuel in oxidizing atmospheres PhD thesis. California Institute of Technology; 1955.
[65] Maqua C, Castanet G, Grisch F, Lemoine F, Kristyadi T, Sazhin SS. Monodisperse droplet heating and evaporation: experimental study and modelling. Int J Heat Mass Transfer 2008;51(15–16):3932–45. http://dx.doi.org/10.1016/j.ijheatmasstransfer.2007.12.011.
[66] Jenny P, Roekaerts D, Beishuizen N. Modeling of turbulent dilute spray combustion. Prog Energy Combust Sci 2012;38(6):846–87. http://dx.doi.org/10.1016/j.pecs.2012.07.001.